Available online at www.sciencedirect.com

ScienceDirect

IFAC PapersOnLine CONFERENCE PAPER ARCHIVE

IFAC PapersOnLine 56-2 (2023) 451–457

Complex-Variable Sliding-Mode Control of Instantaneous Complex Energy and Power for Grid-Tied Inverter ⋆

Gerardo Tapia-Otaegui *, **Sebastián Gómez Jorge** **, **Jorge A. Solsona** **, **Ana Susperregui** *, **M. Itsaso Martínez** *, **Claudio A. Busada** **

* *University of the Basque Country UPV/EHU, Dept. of Automatic Control and Systems Engineering, Faculty of Engineering–Gipuzkoa, 20018 Donostia, Spain (e-mail: gerardo.tapia@ehu.eus)*

** *Instituto de Investigaciones en Ingeniería Eléctrica (CONICET-UNS) and Dpto. de Ingeniería Eléctrica y de Computadoras–Universidad Nacional del Sur, 8000 Bahía Blanca, Argentina (e-mail: sebastian.gomezjorge@uns.edu.ar)*

Abstract: A complex-variable sliding-mode control (SMC) algorithm is proposed to govern inverters interfacing renewable energy sources (RESs) with the electrical grid. It is conceived to control the instantaneous energy stored in the passive components of the system and its rate of change, as well as the instantaneous reactive energy and power exchanged with the grid. The stability of the resulting closed-loop system is analyzed, and tuning of the designed SMC algorithm is also tackled. In addition, the design and tuning of a nonlinear observer estimating the renewable power supplied to the DC link are addressed. The overall control scheme obtained by combining the proposed complex-variable SMC algorithm with such observer is assessed in simulation, demonstrating its outstanding tracking performance and high robustness in presence of large parameter variations.

Keywords: Complex variables, energy control, inverters, observers, power control, renewable energy systems, robustness, stability analysis, sliding-mode control.

1. INTRODUCTION

Due mainly to the requirement of modifying the waveforms provided by generators based on non-conventional renewable energy sources (RESs), nowadays, power converters are being widely used as an interface between the electrical grid and this type of generators. When it is pursued to inject power to the grid at the point of common coupling (PCC), as in this work, power converters are commonly used together with inductive grid filters, so that the whole set behaves as an alternating current source. Nonetheless, voltage sources can also be built based on power converters. Aside from grid integration of renewable energy —Carrasco et al. (2006); Baroudi et al. (2007); Bouzid et al. (2015)—, those current and voltage sources are used in many other applications, such as, for instance, those aimed at improving the quality of the grid power, like active power filters, unified power quality conditioners or high-voltage direct current transmission —Singh et al. (1999, 2009); Chawda et al. (2020); Hannan et al. (2018).

In this context, the model of the set comprising the power converter and the grid filter may be formulated in terms of the input power and the power to be injected by applying the instantaneous power theory —Akagi et al. (2017). Furthermore, if active and reactive powers are grouped into a single complex variable, named instantaneous complex power, the instantaneous complex power theory arises —Milanez and Miskulim (1993); Tedeschi et al. (2007); Lorduy et al. (2009)—, which is intended to tackle scenarios where the application of Budeanu's theory is limited —Jeltsema (2015). Accordingly, the system model may be compactly expressed in complex-variable format, which favors the design of complex-variable control systems.

Along these lines, linear complex-variable controllers have been proposed, among others, in Dòria-Cerezo and Bodson (2016), Dòria-Cerezo et al. (2019) and Golestan et al. (2019). However, as the average-value model of power converters is highly nonlinear, nonlinear controllers can lead to better performance when large excursions of the state variables occur due to load variations or abrupt set-point changes. Recent applications of nonlinear control systems for the rectifier case are provided in Gui et al. (2021) and Solsona et al. (2021b), the latter being formulated in complex variables. Regarding the inverter case, nonlinear complex-variable control schemes are designed in Solsona et al. (2020) and Solsona et al. (2021a) by combining feedback linearization with, respectively, state feedback and sliding-mode control (SMC). In contrast, being the SMC intrinsically nonlinear, the feedback linearization stage is

⋆ Co-financed by the MICIN/AEI/10.13039/501100011033 (project code PID2020-115484RA-I00), by the Basque Government under research grant IT1644-22, by the Universidad Nacional del Sur (UNS), and by the Consejo Nacional de Investigaciones Científicas y Técnicas (CONICET).

10.1016/j.ifacol.2023.10.1609

eluded in this work by proposing a direct complex-variable SMC strategy —Dòria-Cerezo et al. (2021).

Unlike the most common practice, the switching variable selected to that end is nonlinear, as it involves the energy stored in the passive components of the system. This allows treating the closed-loop dynamics of the DC-link voltage together with those of the grid current. In this way, the former are not deliberately forced to be around an order of magnitude slower than the latter, as is typically done when cascading the DC-link voltage control-loop to that of the grid current. As a result, the closed-loop dynamics of the DC-link voltage are greatly improved, thereby substantially dampening the charging/discharging transients experienced by the DC-link capacitor. Besides leading to a more direct and efficient power transfer from the RES to the electrical grid, this opens the door to a downsizing of such capacitor.

The rest of the paper is organized as follows. Based on the complex-variable model of the grid-tied inverter provided in Section 2, Section 3 presents a complex-variable SMC algorithm designed to track instantaneous complex energy and power references. The aspects of stability and tuning are also addressed in Section 3. An input power observer is designed in Section 4. Section 5 evaluates in simulation the control scheme resulting from integrating such observer in the proposed SMC strategy. Finally, conclusions are drawn in Section 6.

2. COMPLEX-VARIABLE MODEL OF THE GRID-TIED INVERTER

If the three-phase i_{abc} grid current, v_{abc} grid voltage and μ_{abc} modulation index are brought to the stationary α-β reference frame by applying the Clarke's transform, each of them may be represented by a single complex variable as $i = i_\alpha + ji_\beta$, $v = v_\alpha + jv_\beta$ and $\mu = \mu_\alpha + j\mu_\beta$. As a result, the dynamics of the grid-tied inverter in Fig. 1 may be expressed compactly as follows —Solsona et al. (2020)—:

$$L\dot{i} = \mu v_C - v - Ri \tag{1}$$

$$\dot{E}_C = P_i - v_C \Re\{\tilde{\mu} i\}, \tag{2}$$

where $\Re\{\cdot\}$ and $\tilde{\cdot}$ refer, respectively, to the real part and the conjugate of the involved complex variable, L and R are the grid-filter inductance and resistance, v_C is the DC-link voltage, $E_C = Cv_C^2/2$ represents the energy stored in the DC-link capacitor of C capacitance, and P_i corresponds to the input power supplied to the DC link by some RES. This power transfer is modeled as a controlled current source, with P_i being constant in steady state.

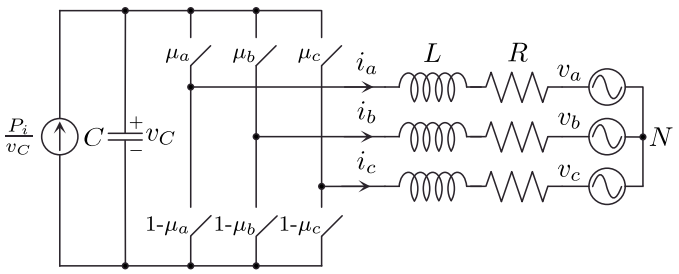

Fig. 1. Conceptual model of an inverter connecting a RES with the grid

3. COMPLEX-VARIABLE SMC ALGORITHM

3.1 Control Objectives and Switching Variable Selection

It is proposed to control the instantaneous complex energy

$$\xi_1 = E_C + \tfrac{1}{2}L|i|^2 + j\int_0^t Q(\tau)d\tau, \tag{3}$$

where $Q = \Im\{v\tilde{i}\}$ is the grid reactive power and $\Im\{\cdot\}$ denotes the imaginary part of the complex variable it accompanies. Note that the real part of ξ_1 represents the instantaneous energy stored in both C and L, which is a direct consequence of the active power transfer from the DC link to the grid.

It is also sought to control the instantaneous complex power corresponding to the time derivative of ξ_1, which may be computed by considering the power balance as

$$\xi_2 = \dot{\xi}_1 = P_i - R|i|^2 - P + jQ = P_i - R|i|^2 - \tilde{v}i, \tag{4}$$

with $P = \Re\{v\tilde{i}\}$ being the grid active power. Accordingly, the real part of ξ_2 represents the rate of change of the energy stored in both C and L.

Consequently, the nonlinear complex switching variable given next is selected:

$$\sigma = \underbrace{\xi_2 - \xi_2^*}_{e_{\xi_2}} + g_1(\underbrace{\xi_1 - \xi_1^*}_{e_{\xi_1}}) + g_2\int_0^t [\xi_1(\tau) - \xi_1^*(\tau)]d\tau, \tag{5}$$

where ξ_1^* and ξ_2^* represent the reference values for ξ_1 and ξ_2, respectively, and g_1 and g_2 are real positive constants defining the dynamics according to which errors e_{ξ_1} and e_{ξ_2} are driven to zero once the sliding regime is achieved.

3.2 Design of the Control Law

In order to transfer the system dynamics to the switching variable, the time derivative of (5) is first taken, yielding

$$\dot{\sigma} = \dot{e}_{\xi_2} + g_1 e_{\xi_2} + g_2 e_{\xi_1}. \tag{6}$$

Similarly, taking the time derivative of (4) and replacing the resulting expression in (6) produces

$$\dot{\sigma} = \dot{P}_i - \dot{\xi}_2^* - 2R\Re\{i\dot{\tilde{i}}\} + g_1 e_{\xi_2} + g_2 e_{\xi_1} - \dot{\tilde{v}}i - \tilde{v}\dot{i}. \tag{7}$$

Now, substituting the two instances of $\dot{i}$ in (7) by (1) and considering that, by virtue of (2), $v_C\Re\{\tilde{\mu}i\} = P_i - \dot{E}_C$, it turns out that

$$\dot{\sigma} = \dot{P}_i - \dot{\xi}_2^* - \tfrac{2R}{L}\Big(P_i - \dot{E}_C - \Re\{v\tilde{i}\} - R|i|^2\Big) + g_1 e_{\xi_2} + g_2 e_{\xi_1} - \dot{\tilde{v}}i + \tfrac{R}{L}\tilde{v}i + \tfrac{1}{L}|v|^2 - \tfrac{1}{L}v_C\tilde{v}\mu. \tag{8}$$

Finally, if it is assumed that the three-phase grid voltage is purely sinusoidal and balanced, it can be represented as $v = |v|e^{j\omega t}$, with ω and t denoting, respectively, the frequency of the grid voltage and time. As a consequence,

$$\dot{\tilde{v}} = -j\omega\tilde{v}, \tag{9}$$

which, once replaced in (8), gives rise to

$$\dot{\sigma} = \dot{P}_i - \dot{\xi}_2^* - \tfrac{2R}{L}\Big(P_i - \dot{E}_C - \Re\{v\tilde{i}\} - R|i|^2\Big) + g_1 e_{\xi_2} + g_2 e_{\xi_1} + \big(\tfrac{R}{L} + j\omega\big)\tilde{v}i + \tfrac{1}{L}|v|^2 - \tfrac{1}{L}v_C\tilde{v}\mu, \tag{10}$$

evidencing that the system to be controlled is of relative order one, as control signal μ appears explicitly after having taken the first time derivative of σ.

A standard —first-order— SMC law of the following format is accordingly adopted:

$$\mu = \mu_{eq} + K\frac{\sigma}{|\sigma|};\ K = |K|\angle\arg(K) \in \mathbb{C}, \tag{11}$$

where μ_{eq} is the equivalent control term, which can be derived by zeroing $\dot{\sigma}$ in (10) and subsequently solving for μ. As a result,

$$\mu_{eq} = \frac{L\Big(\dot{P}_i - \dot{\xi}_2^* + g_1 e_{\xi_2} + g_2 e_{\xi_1}\Big) + (R + L\omega j)\tilde{v}i + |v|^2}{v_C\tilde{v}} - 2R\frac{P_i - \dot{E}_C - \Re\left\{v\tilde{i}\right\} - R|i|^2}{v_C\tilde{v}}. \tag{12}$$

Although expression (12) might seem complicated, μ_{eq} is perfectly calculable. Indeed, taking into account that, in most applications, the energy stored in the DC-link capacitor turns out to be much greater than that stored in the grid-filter inductance, the ξ_1^*, ξ_2^* and $\dot{\xi}_2^*$ reference values in (12) may be computed as follows:

$$\xi_1^* = \tfrac{1}{2}Cv_C^{*2} + j\int_0^t Q^*(\tau)d\tau \tag{13}$$

$$\xi_2^* = \dot{\xi}_1^* = Cv_C^*\dot{v}_C^* + jQ^* \tag{14}$$

$$\dot{\xi}_2^* = C\big(\dot{v}_C^{*2} + v_C^*\ddot{v}_C^*\big) + j\dot{Q}^*, \tag{15}$$

with v_C^* and Q^* being, respectively, the reference values for v_C and Q. In order to avoid undesired transients, the $\dot{v}_C^*$, $\ddot{v}_C^*$ and $\dot{Q}^*$ reference values in (14) and (15) may be defined by considering that both v_C^* and Q^* can either remain constant or vary smoothly —following ramps, for example— from one constant value to another.

Regarding the rest of the variables involved in (12), v_C, v and i are directly measured in this work, while P_i and $\dot{P}_i$ are provided by the input power observer proposed in Section 4. In contrast, derivation of $\dot{E}_C$ is not straightforward, but it may be roughly approximated by

$$\dot{E}_C = \frac{d\left(Cv_C^2/2\right)}{dt} = Cv_C\dot{v}_C \approx Cv_C\dot{v}_C^* = \hat{\dot{E}}_C, \tag{16}$$

which is equivalent to assuming that $\dot{v}_C$ closely tracks its $\dot{v}_C^*$ reference value. Consequently, the error arising from this approximation turns out to be

$$\dot{E}_C - \hat{\dot{E}}_C = Cv_C\left(\dot{v}_C - \dot{v}_C^*\right). \tag{17}$$

Similarly, the ω in (12) is simply replaced by ω_N, with subscript N standing for nominal value hereafter. The inaccuracies to which approximations/estimations of these and other variables lead, together with parameter mismatches, unmodeled dynamics and external disturbances, adversely affect calculation of μ_{eq}. Nonetheless, the robustness of the overall control algorithm in (11) is not compromised, since such robustness rests on its switching term.

3.3 Stability Analysis and Tuning

Aiming at selecting the complex gain K in (11), a stability analysis is carried out based on Lyapunov function

$$V = \tfrac{1}{2}|\sigma|^2 = \tfrac{1}{2}\sigma\tilde{\sigma}, \tag{18}$$

whose time derivative, given by

$$\dot{V} = \tfrac{1}{2}\left(\dot{\sigma}\tilde{\sigma} + \sigma\dot{\tilde{\sigma}}\right) = \Re\left\{\tilde{\sigma}\dot{\sigma}\right\}, \tag{19}$$

must be kept negative to ensure convergence of σ to zero and, consequently, achievement of the sliding regime.

Aiming at evaluating the effect of K on $\dot{V}$, (10) is first replaced in (19), yielding

$$\dot{V} = \Re\Bigg\{\tilde{\sigma}\Bigg[\dot{P}_i - \dot{\xi}_2^* - \tfrac{2R}{L}\Big(P_i - \dot{E}_C - \Re\big\{v\tilde{i}\big\} - R|i|^2\Big) + g_1 e_{\xi_2} + g_2 e_{\xi_1} + \big(\tfrac{R}{L} + j\omega\big)\tilde{v}i + \tfrac{1}{L}|v|^2 - \tfrac{1}{L}v_C\tilde{v}\mu\Bigg]\Bigg\}. \tag{20}$$

Now, if it is assumed that the $\dot{E}_C$ in (12) is approximated as in (16) and ω is replaced by ω_N in (12), substitution of (11) and (12) into (20) leads to

$$\dot{V} = \tfrac{1}{L}\Re\left\{\tilde{\sigma}F - v_C\tilde{v}K|\sigma|\right\}, \tag{21}$$

with perturbation F being

$$F = 2RCv_C\left(\dot{v}_C - \dot{v}_C^*\right) + jL\left(\omega - \omega_N\right)v\tilde{i}. \tag{22}$$

Notice that the errors made when approximating the $\dot{E}_C$ —see (17)— and the ω present in (12) are respectively responsible for the real and imaginary parts of F. Yet, it must be highlighted that, in general, F will be a complex variable dependent on all estimation errors, parameter deviations, unmodeled dynamics and disturbances present when calculating the equivalent control term in (12).

By expressing σ and v in polar form as $\sigma = |\sigma|\angle\arg(\sigma)$ and $v = |v|\angle\arg(v)$, (21) may be rewritten as

$$\dot{V} = \tfrac{1}{L}\left(\Re\{F\}\cos\left[\arg(\sigma)\right] + \Im\{F\}\sin\left[\arg(\sigma)\right]\right)|\sigma| - \tfrac{1}{L}v_C\,|v|\,|K|\cos\left[\arg(K) - \arg(v)\right]|\sigma|. \tag{23}$$

Given that $\dot{V} < 0$ must be fulfilled to guarantee convergence of σ to zero, (23) evidences that forcing

$$\arg(K) = \arg(v) \tag{24}$$

favors achievement of the sliding regime, as it causes the last term in (23) to be as negative as possible. Thus, under such assumption, if F is expressed in polar form as $F = |F|\angle\arg(F)$, (23) becomes

$$\dot{V} = \tfrac{1}{L}\left(|F|\cos\left[\arg(F) - \arg(\sigma)\right] - v_C\,|v|\,|K|\right)|\sigma| \tag{25}$$

when applying the difference identity for cosine.

Now, considering the worst-case scenario in which $|F|$ equals its upper bound $|F|_{max}$, $\arg(F) = \arg(\sigma)$, and v_C and $|v|$ are at their respective lower bounds, $v_{C_{min}}$ and $|v|_{min}$, (25) can be majored to yield

$$\dot{V} \leq \tfrac{1}{L}\left(|F|_{max} - v_{C_{min}}\,|v|_{min}\,|K|\right)|\sigma|, \tag{26}$$

hence revealing that selection of $|K|$ as

$$|K| > \frac{|F|_{max}}{v_{C_{min}}\,|v|_{min}} \tag{27}$$

would ensure $\dot{V} < 0$ at all times.

In practice, taking into account that the power-invariant Clarke's transform is adopted in this work, $|\mu|$ should not exceed $|\mu|_{max} = \sqrt{2}/2$ if it is intended, for example, to apply space-vector modulation (SVM). Consequently, by virtue of (11), it would not make sense to select $|K| > |\mu|_{max}$ even in the most demanding case that $|\mu_{eq}|$ equals zero.

Finally, in order to tune the g_1 and g_2 parameters present in both σ and μ_{eq}, it is recalled that the closed-loop dynamics while in the sliding regime coincide with those resulting from driving the system with $\mu = \mu_{eq}$ in absence of any uncertainty —either parametric or unstructured—,

estimation error and disturbance. Now, given that application of equivalent control under such ideal conditions leads to $\dot{\sigma} = 0$, this is precisely the expression describing the closed-loop dynamics while in the sliding regime. Accordingly, if (6) is zeroed and subsequently expressed in state-space form, it becomes

$$\begin{bmatrix} \dot{e}_{\xi_1} \\ \dot{e}_{\xi_2} \end{bmatrix} = \underbrace{\begin{bmatrix} 0 & 1 \\ -g_2 & -g_1 \end{bmatrix}}_{\mathbf{A}} \begin{bmatrix} e_{\xi_1} \\ e_{\xi_2} \end{bmatrix}, \tag{28}$$

hence evidencing that, if non-zero, both e_{ξ_1} and e_{ξ_2} will vanish to zero as dictated by the eigenvalues of matrix $\mathbf{A}$, whose characteristic polynomial is given by

$$p^2 + g_1 p + g_2 = 0, \tag{29}$$

with $p = d/dt$ representing the Laplace operator.

Parameters g_1 and g_2 may then be tuned so that characteristic polynomial (29) is identical to an objective characteristic polynomial given by $p^2 + 2\zeta\omega_n p + \omega_n^2$. By doing so, possible errors in both ξ_1 and ξ_2 will converge to zero showing a $t_s = 4.6/(\zeta\omega_n)$ settling time —according to the 1% criterion— and a ζ damping coefficient. The latter is therefore achieved simply by forcing

$$g_1 = 2\zeta\omega_n;\ g_2 = \omega_n^2. \tag{30}$$

4. INPUT POWER OBSERVER

It is considered that the RES supplying the P_i input power depicted in Fig. 1 can be assimilated to a constant power source (CPS), which is, for example, the case for converters —provided with maximum power-point tracking (MPPT) algorithms— draining power from wind turbines or photovoltaic panels. Consequently, the constant input power assumption performs sufficiently well for the majority of cases. Nonetheless, given that knowledge of $\dot{P}_i$ is required to compute equivalent control (12), the input power dynamics are eventually represented by

$$\dot{P}_i = m \tag{31}$$

$$\dot{m} = 0. \tag{32}$$

Accordingly, based on (2), (31) and (32), the observer given next is proposed:

$$\dot{\hat{E}}_C = \hat{P}_i - v_C \Re\{\tilde{\mu} i\} + k_1 e_{E_C} \tag{33}$$

$$\dot{\hat{P}}_i = \hat{m} + k_2 e_{E_C} \tag{34}$$

$$\dot{\hat{m}} = k_3 e_{E_C}, \tag{35}$$

where $e_{E_C} = E_C - \hat{E}_C$, and $k_l \in \mathbb{R}$; $l = 1, 2, 3$. Hence, subtraction of (33), (34) and (35) from, respectively, (2), (31) and (32) yields the following linear state-space description for the estimation error:

$$\begin{bmatrix} \dot{e}_{E_C} \\ \dot{e}_{P_i} \\ \dot{e}_m \end{bmatrix} = \underbrace{\begin{bmatrix} -k_1 & 1 & 0 \\ -k_2 & 0 & 1 \\ -k_3 & 0 & 0 \end{bmatrix}}_{\mathbf{A}_{P_i}} \begin{bmatrix} e_{E_C} \\ e_{P_i} \\ e_m \end{bmatrix}, \tag{36}$$

where $e_{P_i} = P_i - \hat{P}_i$ and $e_m = m - \hat{m}$.

The tuning formulas for k_1, k_2 and k_3 are derived by equating the characteristic polynomial associated to matrix $\mathbf{A}_{P_i}$, given by $p^3 + k_1 p^2 + k_2 p + k_3$, to the 3rd-degree target characteristic polynomial

$$\left(p^2 + 2\zeta_{P_i}\omega_{n_{P_i}} p + \omega_{n_{P_i}}^2\right)\left(p + \kappa\zeta_{P_i}\omega_{n_{P_i}}\right). \tag{37}$$

As a result,

$$k_1 = (2 + \kappa)\,\zeta_{P_i}\omega_{n_{P_i}} \tag{38}$$

$$k_2 = \left(1 + 2\kappa\zeta_{P_i}^2\right)\omega_{n_{P_i}}^2 \tag{39}$$

$$k_3 = \kappa\zeta_{P_i}\omega_{n_{P_i}}^3. \tag{40}$$

Note that κ may be selected so that the roots of the 2nd-degree polynomial in (37) are dominant and, consequently, possible estimation errors vanish to zero exhibiting a $t_{s_{P_i}} = 4.6/\left(\zeta_{P_i}\omega_{n_{P_i}}\right)$ settling time, according to the 1% criterion, as well as a ζ_{P_i} damping coefficient.

5. SIMULATION RESULTS

Aiming at validating the global control scheme that combines the SMC algorithm and the observer described, respectively, in Sections 3 and 4, a simulation study was carried out on a grid-tied inverter model whose parameters are collected in Table 1. An average-value model was adopted to represent the inverter itself. This way, any chatter observable in simulation tests was directly attributable to the SMC, since chattering due to transistor switching was non-existent. Simulation tests were run starting from a steady-state scenario in which $v_C = v_C^* = 650$ V ($E_C = E_C^* = 63.375$ J), $P_i = 0$ W, $Q = Q^* = 0$ VAr, $|v| = |v_N|$ and $\omega = \omega_N$. All the events caused throughout such tests are summarized in Table 2.

Table 1. Parameters of the grid-tied inverter

Parameter	Value
C	300 μF
L	5 mH
R	0.1 Ω
$\lvert v_N \rvert$	$\sqrt{3}\,220$ V
ω_N	$2\pi 50$ rad/s

Table 2. Events triggered during simulations

Time range/instant	Event
0.01–0.02 s	P_i ramps up from 0 to 2 kW
0.05–0.06 s	v_C^* ramps up from 650 to 700 V (E_C^* ramps up from 63.375 to 73.5 J)
0.15–0.16 s	Q^* ramps up from 0 to 1 kVAr
0.2 s	ω steps up from ω_N to $1.05\omega_N$
0.25 s	ω steps down from $1.05\omega_N$ to ω_N
0.3 s	$\lvert v \rvert$ steps down from $\lvert v_N \rvert$ to $0.8\lvert v_N \rvert$
0.35 s	$\lvert v \rvert$ steps up from $0.8\lvert v_N \rvert$ to $\lvert v_N \rvert$

On the other hand, the tuning equations in (30) and (38)–(40) were applied to derive the values for the parameters of the SMC algorithm and the observer. Furthermore, the $K\sigma/|\sigma|$ switching control term was replaced by $K\sigma/(|\sigma| + \delta)$, with δ being a small positive scalar. In doing so, the discontinuity exhibited by the complex-variable version of the sign function at $\sigma = 0$ was smoothed by approximating it to an arbitrarily close but continuous sigmoid-like function. This approach allows mitigating possible chatter, as reasoned, for example, in Edwards and Spurgeon (1998). Both the defined specifications and the parameter values resulting from such specifications are displayed in Table 3.

Table 3. Specifications and parameter values

Specifications	Parameter values
SMC algorithm	
$t_s = 10$ ms; $\zeta = 0.707$	$g_1 = 920$
$\omega_n = 650.64$ rad/s	$g_2 = 423.33\times10^3$
SVM modulation	$K = \sqrt{2}/2$
Chatter mitigation	$\delta = 3.5$
Input power observer	
$t_{s_{P_i}} = 2$ ms; $\zeta_{P_i} = 0.707$	$k_1 = 9.2\times10^3$
$\omega_{n_{P_i}} = 3.25\times10^3$ rad/s	$k_2 = 31.74\times10^6$
$\kappa = 2$	$k_3 = 48.68\times10^9$

5.1 Performance Evaluation

Fig. 2 shows the main simulation results illustrating the performance of the observer-based SMC scheme. As evidenced by Fig. 2(a), 2(c) and 2(d), $\Re\{\xi_1^*\}$, $\Re\{\xi_2^*\}$ and Q^* are all closely tracked despite the different events listed in Table 2. Indeed, $\Re\{\xi_1\}$, $\Re\{\xi_2\}$ and Q practically overlap their respective reference signals for the most part. Slight deviations from $\Re\{\xi_2^*\}$, due to the dynamics of the input power observer, are noticeable in Fig. 2(c) both at the beginning and at the end of the P_i ramp-up. Similarly, as a result of having assumed that $|v|$ is constant when deriving (9), the 20% drop in the grid voltage and its subsequent recovery also lead to very short-duration deviations from $\Re\{\xi_2^*\}$ and Q^*. In contrast, although ω is approximated by ω_N, the two abrupt changes in the grid frequency have no noticeable effect. Note also that, in spite of the near-perfect tracking of $\Re\{\xi_1^*\}$, a negligible error in the DC-link voltage —not exceeding 0.6 V in the worst case— is visible in Fig. 2(b). The latter is due to the fact that $\Re\{\xi_1^*\}$ is computed in (13) by disregarding the energy stored in L.

Concerning estimation of the input power, Fig. 2(e) reflects that the initial ramp-up of P_i is tracked by the observer with the expected dynamics, presenting a minimum short-duration overshoot when P_i reaches its final value. The three-phase grid current is displayed in Fig. 2(f), where the transients and peak value variations following most of the test events —excluding the two sudden frequency variations— are clearly identifiable and evolve as expectable. Finally, the three-phase modulation index leading to the preceding results is observable in Fig. 2(g).

5.2 Evaluation of Robustness

With the aim of assessing the robustness of the proposed observer-based SMC scheme under parameter variations, the simulation study was repeated for 50% deviations in the L and C of the grid-tied inverter with respect to their nominal values, provided in Table 1. However, those nominal values were deliberately kept within the SMC algorithm and the observer.

Fig. 3 collects the main results corresponding to the four possible scenarios presenting mismatches in both L and C, compared to those obtained in absence of parameter deviations. In summary, apart from displaying the impact of those substantial parameter deviations on the control dynamics —see Fig. 3(a) to 3(d)— and the estimation error —see Fig. 3(e)—, Fig. 3 shows that the performance of the proposed control scheme remains highly satisfactory

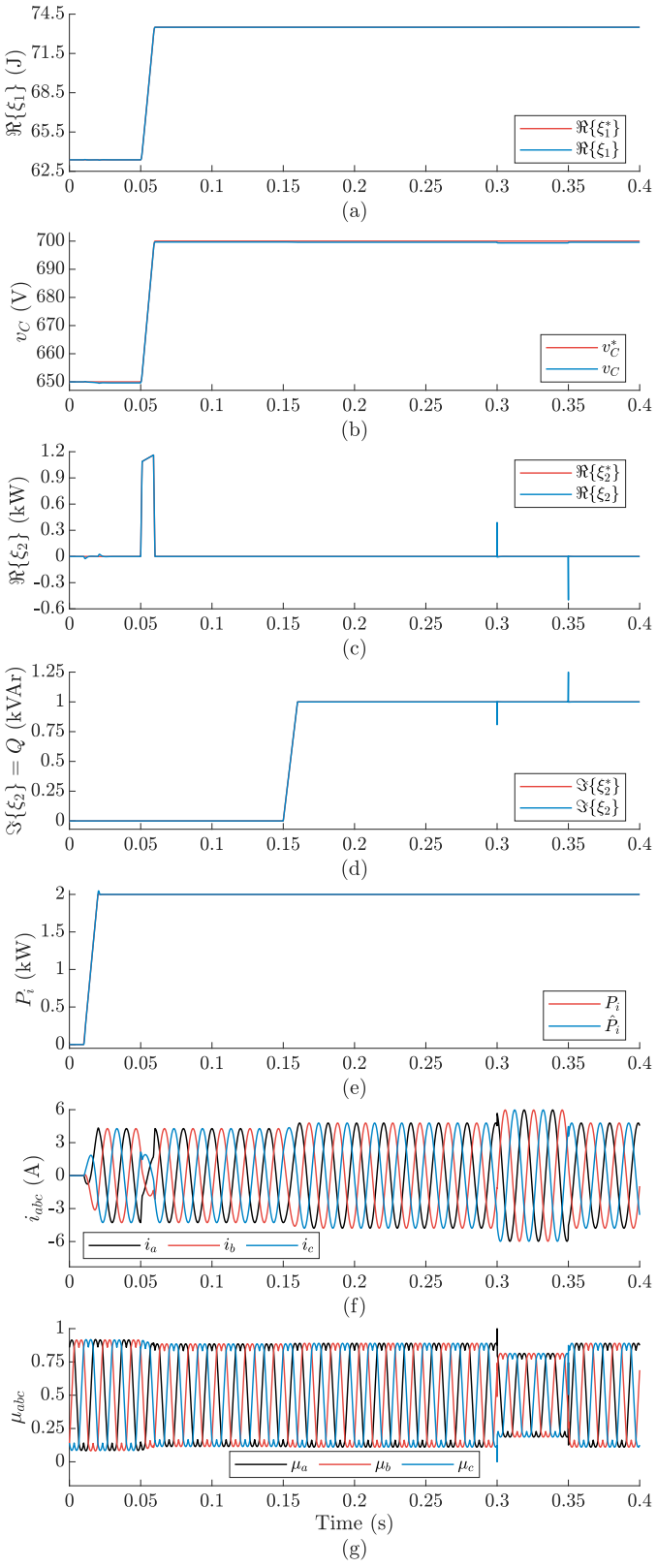

Fig. 2. Performance of the SMC algorithm. (a) Instantaneous energy stored in C and L. (b) DC-link voltage. (c) Rate of change of the energy stored in C and L. (d) Grid reactive power. (e) Input power and its estimate. (f) Three-phase grid current. (g) Three-phase modulation index

and practically unchanged. It is worth noting, however, that, as expectable, mismatches in C cause input power estimation errors to appear during the ramp-up of P_i —refer to Fig. 3(e)—, the transients of such errors being less damped as C increases.

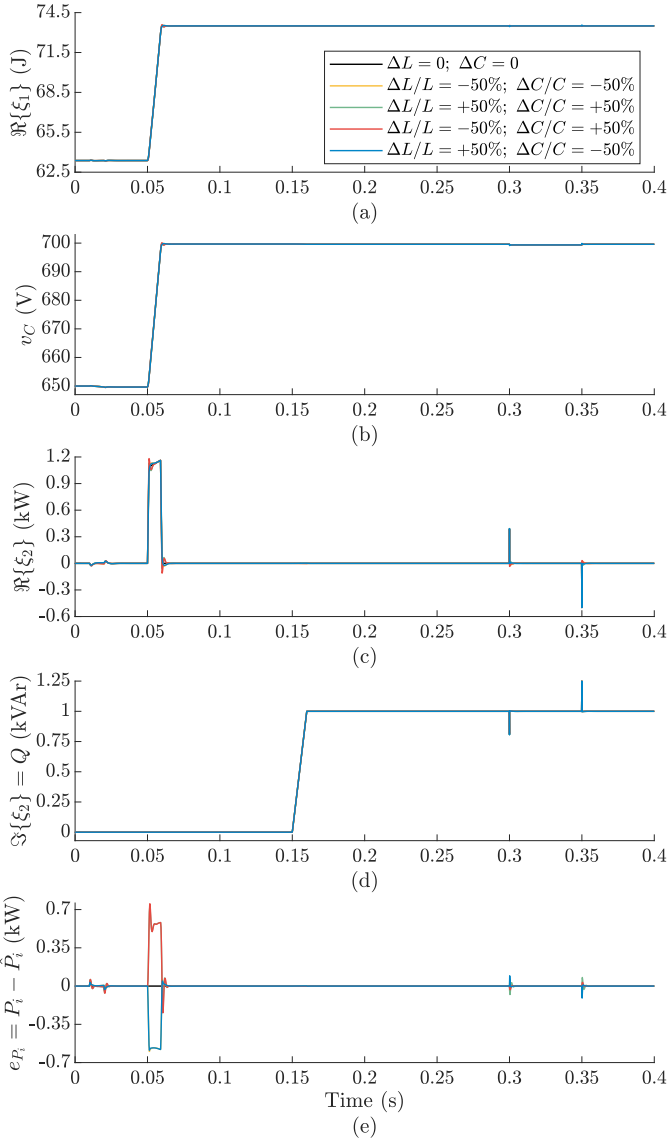

Fig. 3. Robustness under 50% mismatches in both C and L. (a) Instantaneous energy stored in the system. (b) DC-link voltage. (c) Rate of change of the energy stored in the system. (d) Grid reactive power. (e) Input power estimation error

6. CONCLUSION

A complex-variable SMC algorithm, based on a nonlinear switching function, has been designed for inverters interconnecting RESs with the electrical grid. Tuning formulas are derived to adjust it, together with the condition that needs to be met to ensure the stability of the closed-loop system to which it leads. Both the power supplied by the RES and its time derivative, which must be available to the SMC algorithm, are estimated by an observer whose design and tuning are also tackled. As a result of controlling the energy stored in the DC link and the grid filter, as well as its rate of change, the dynamics of both the DC-link voltage and the grid current are treated together. By doing so, it is avoided to cascade a significantly slower DC-link voltage control-loop to that of the grid current. The resulting observer-based control scheme exhibits superior tracking performance despite large parameter changes and estimation error.

REFERENCES

Akagi, H., Watanabe, E.H., and Aredes, M. (2017). *Instantaneous Power Theory and Applications to Power Conditioning*. John Wiley & Sons.

Baroudi, J.A., Dinavahi, V., and Knight, A.M. (2007). A review of power converter topologies for wind generators. *Renew. Energy*, 32(14), 2369–2385.

Bouzid, A.M., Guerrero, J.M., Cheriti, A., Bouhamida, M., Sicard, P., and Benghanem, M. (2015). A survey on control of electric power distributed generation systems for microgrid applications. *Renew. Sustain. Energy Rev.*, 44, 751–766.

Carrasco, J.M., Garcia Franquelo, L., Bialasiewicz, J.T., Galván, E., Portillo Guisado, R.C., Martín Prats, M.Á., León, J.I., and Moreno-Alfonso, N. (2006). Power-electronic systems for the grid integration of renewable energy sources: A survey. *IEEE Trans. Ind. Electron.*, 53(4), 1002–1016.

Chawda, G.S., Shaik, A.G., Mahela, O.P., Padmanaban, S., and Holm-Nielsen, J.B. (2020). Comprehensive review of distributed FACTS control algorithms for power quality enhancement in utility grid with renewable energy penetration. *IEEE Access*, 8, 107614–107634.

Dòria-Cerezo, A. and Bodson, M. (2016). Design of controllers for electrical power systems using a complex root locus method. *IEEE Trans. Ind. Electron.*, 63(6), 3706–3716.

Dòria-Cerezo, A., Olm, J.M., Biel, D., and Fossas, E. (2021). Sliding modes in a class of complex-valued nonlinear systems. *IEEE Trans. Autom. Control*, 66(7), 3355–3362.

Dòria-Cerezo, A., Serra, F.M., and Bodson, M. (2019). Complex-based controller for a three-phase inverter with an LCL filter connected to unbalanced grids. *IEEE Trans. Power Electron.*, 34(4), 3899–3909.

Edwards, C. and Spurgeon, S.K. (1998). *Sliding Mode Control: Theory and Applications*. Taylor & Francis, London, UK.

Golestan, S., Guerrero, J.M., Vasquez, J.C., and Abusorrah, A.M. (2019). Modeling and tuning of adaptive complex current controller for three-phase grid-interfaced power converters. In *2019 IEEE Int. Conf. Environ. Elect. Eng./2019 IEEE Ind. Commercial Power Syst. Eur. (EEEIC/I&CPS Europe)*, 1–6.

Gui, Y., Blaabjerg, F., Wang, X., Bendtsen, J.D., Yang, D., and Stoustrup, J. (2021). Improved DC-link voltage regulation strategy for grid-connected converters. *IEEE Trans. Ind. Electron.*, 68(6), 4977–4987.

Hannan, M.A., Hussin, I., Ker, P.J., Hoque, M.M., Hossain Lipu, M.S., Hussain, A., Rahman, M.S.A., Faizal, C.W.M., and Blaabjerg, F. (2018). Advanced control strategies of VSC based HVDC transmission system: Issues and potential recommendations. *IEEE Access*, 6, 78352–78369.

Jeltsema, D. (2015). Budeanu's concept of reactive and distortion power revisited. In *2015 Int. School Nonsinusoidal Currents and Compensation (ISNCC)*, 1–6.

Lorduy, A., Lazaro, A., Fernandez, C., Quesada, I., and Barrado, A. (2009). Novel simplified controller for three phase grid connected inverter based on instantaneous complex power. In *2009 24th Annu. IEEE Appl. Power Electron. Conf. Expo.*, 1306–1312.

Milanez, D.L. and Miskulim, M.S. (1993). The instantaneous complex power applied to three-phase machines. In *Conf. Rec. 1993 IEEE Ind. Appl. Conf. 28th IAS Annu. Meet.*, vol. 1, 171–176.

Singh, B., Al-Haddad, K., and Chandra, A. (1999). A review of active filters for power quality improvement. *IEEE Trans. Ind. Electron.*, 46(5), 960–971.

Singh, B., Saha, R., Chandra, A., and Al-Haddad, K. (2009). Static synchronous compensators (STATCOM): A review. *IET Power Electron.*, 2(4), 297–324.

Solsona, J.A., Gomez Jorge, S., and Busada, C.A. (2020). A nonlinear control strategy for a grid-tie inverter that injects instantaneous complex power to the grid. In *2020 IEEE Int. Conf. Ind. Technol. (ICIT)*, 895–900.

Solsona, J.A., Gomez Jorge, S., Busada, C.A., Tapia-Otaegui, G., Susperregui, A., and Martínez, M.I. (2021a). Control de un inversor autosincronizado que inyecta potencia instantánea compleja en la red eléctrica. In *Anales de Trabajos del RPIC 2021: XIX Reunión de Trabajo en Procesamiento de la Información y Control*, 1–6.

Solsona, J.A., Gomez Jorge, S., Leon, A.E., and Busada, C.A. (2021b). Instantaneous complex power control of a grid-tied VSC supplying a constant power load. *IEEE Trans. Power Electron.*, 36(3), 3591–3599.

Tedeschi, E., Tenti, P., and Mattavelli, P. (2007). Cooperative operation of active power filters by instantaneous complex power control. In *2007 7th Int. Conf. Power Electron. Drive Syst.*, 555–561.